Analysis of Flame Curvature Evolution in a Turbulent Premixed Bluff Body Burner

Cifuentes, Luis; Dopazo, Cesar; Sandeep, Anurag; Chakraborty, Nilanjan; Kempf, Andreas

DOI: https://doi.org/10.1063/1.5044525

URN: urn:nbn:de:hbz:464-20190122-141212-8

Link: https://duepublico.uni-duisburg-essen.de:443/servlets/DocumentServlet?id=47985

Source: **Authors Accepted Manuscript** (Dated: August 17, 2018). - The final version appeared in "Physics of Fluids 30, 095101 (2018)" and may be found at https://doi.org/10.1063/1.5044525

Analysis of Flame Curvature Evolution in a Turbulent Premixed Bluff Body Burner

Luis Cifuentes,[1,*] Cesar Dopazo,[2] Anurag Sandeep,[1]
Nilanjan Chakraborty,[3] and Andreas Kempf[1,4]

[1]*Institute for Combustion and Gasdynamics (IVG), Chair for Fluid Dynamics, University of Duisburg-Essen, Duisburg 47057, Germany*

[2]*School of Engineering and Architecture - Fluid Mechanics Area, University of Zaragoza, C/ Maria de Luna 3, Zaragoza 50018, Spain*

[3]*School of Mechanical and Systems Engineering, Newcastle University, Claremont Road Newcastle-Upon-Tyne NE1 7RU, UK*

[4]*Center for Nano-Integration Duisburg-Essen (CENIDE), University of Duisburg-Essen, Duisburg 47057, Germany*

(Dated: August 17, 2018)

Abstract

The physical mechanisms responsible for flame curvature evolution of a methane-air premixed flame attached to a bluff-body burner have been investigated using a high-fidelity flame-resolved three-dimensional simulation database. The contributions to the mean curvature generation due to the fluid flow motion and to a combination of flow and flame propagation induced strain rates have been analyzed in detail and dominant contributions in different zones (reactants, flame and products) of the flame have been identified. The effect of fluid flow on the mean curvature evolution is important on the unburned gas side, whereas the flame propagation dominates the mean curvature evolution in the reaction region and towards the hot products. The statistical contributions of the mean curvature transport equation have been analysed in terms of the iso-scalar surface geometry, characterized by the mean and Gauss curvatures. This information has subsequently been used to provide physical insights into the dominant mechanisms of curvature evolution for different flame topologies.

Keywords: flame curvature, iso-scalar non-material surfaces, turbulent premixed flame.

*Electronic address: luis.cifuentes@uni-due.de

I. INTRODUCTION

Turbulent premixed flames are inherently curved supposedly because of flame wrinkling induced by turbulent fluid motion [1]. The curvature of premixed flames plays a key role in analyzing how turbulence affects the local flame propagation rate [1–31], the flame strain rate [6, 9, 16–20], the evolution of the reactive scalar gradient and the evolution of the flame area through flame stretch [18, 23, 32–38]. Markstein [2] introduced a phenomenological model for the burning velocity as a function of the flame front curvature. Clavin and Joulin [3] examined the stability of highly wrinkled premixed flames. Activation energy asymptotics were used to examine concave and convex premixed flames with a radius of curvature comparable to the thickness of the preheat zone [4, 5], aiming to analyse the statistical behaviour of flame stretch and its influence on flame propagation. Based on two-dimensional [6, 8, 10–15, 23] and three-dimensional [7, 16–20, 22, 24, 26, 27, 29] Direct Numerical Simulation (DNS), it has been shown that local flame curvature significantly affects the statistical behaviours of displacement speed $S_d = |\nabla c|^{-1}(Dc/Dt)$ (where c is the reaction progress variable) and its components for both statistically planar [10–18, 22–24, 26, 27, 31] and statistically spherical flames [19, 20, 29, 36]. The curvature dependence of displacement speed has also been reported by experimental analyses [9, 21, 25, 28, 30]. Consumption speed $S_c = -\rho_0^{-1}\int \dot{\omega}\mathbf{n}.d\mathbf{x}$ (where $\dot{\omega}$ is the reaction progress variable, $\mathbf{n}$ is the flame normal vector and ρ_0 is the unburned gas density) [6, 7, 21, 31] is also affected by local flame curvature in premixed turbulent combustion. The correlation between the flame speed and curvature weakens with increasing turbulence intensity [12, 13, 18, 21, 26, 27, 31]. These curvature dependences of flame speeds are affected by the effective Lewis number and turbulence intensity, so that the flame surface temperature becomes a strong function of local flame curvature in the presence of differential diffusion of heat and mass [6, 7, 17, 24, 36]. The molecular diffusion rate contribution to displacement speed can be split into flame normal and tangential components, with the latter being directly proportional to the negative mean curvature [6–8, 10–20, 22–24, 26, 27]. The normal diffusion component of displacement speed also exhibits complex curvature dependence especially for non-unity Lewis number flames and flames with a non-zero global mean curvature [16–20].

The correlation between consumption speed and local flame curvature have been found to be positive (negative) for characteristic Lewis numbers greater (smaller) than unity [7],

and a recent DNS analysis of premixed dodecane/air flames with detailed chemical kinetics shows that the negative correlation between consumption speed and curvature decreases with increasing Karlovitz number Ka [31]. The curvature dependences of displacement speed measurements in a low swirl burner for several H_2/CO mixtures at various flow velocities have shown that the leading edge curvature statistics are a strong function of the turbulence intensity of the flow, but display a weak dependence on fuel composition [30].

In addition to propagation, both dilatation and flame tangential strain rates in premixed flames have been found to be negatively correlated to local curvature [6, 9, 16–23, 26, 27] but the curvature dependence weakens with increasing turbulence intensity [12, 13, 18, 21, 26, 27]. The curvature dependences of displacement speed and tangential strain rate lead to a non-linear curvature dependence of stretch rate, (which includes the tangential strain rates due to the flow and that induced by curvature) [32, 33]. Data from DNS with simple [15] and detailed chemistry [26] has shown that the average stretch due to curvature can play an important role; while most flame area displays a radius of curvature greater than the laminar flame thickness, most stretch occurs in flame elements with higher curvature. The effects of flame stretch on the evolution of flame surface area and the scalar gradient magnitude SDF have been elucidated by Pope [32] and Candel & Poinsot [33] (SDF stands for surface density function and quantifies the local elementary surface/volume ratio [18, 34–37]). Pope [32] described the local geometry of fluid and scalar iso-surfaces by evolution equations in parametric coordinates for the position vector, unit vector normal to the surface, principal curvatures and area stretch factor and derived a transport equation for the SDF. Candel & Poinsot [33] derived the mathematical expression for flame stretch, and evolution equations of flame area, volume and surface to volume ratio. Girimaji and Pope [38] used DNS datasets of isotropic turbulent velocity fields to examine the evolution of surfaces that propagate at a constant velocity, and computed statistical data of tangential strain rate, fluid velocity, characteristic curvature and area of propagating surface elements. It has been demonstrated that the curvature dependences of stretch rate, dilatation rate and tangential strain rate give rise to complex correlations between the terms of the SDF transport equation and curvature [18, 23, 34–36]. These correlations are also affected by the characteristic Lewis number [35], choice of the fuel-air mixture and global mean curvature [36]. Moreover, the effects of curvature on the scalar dissipation rate (SDR) evolution [39] are analogous to those on SDF transport. These curvature dependences of flame displacement speed and

SDF have been found to be of crucial importance in the closures of Flame Surface Density (FSD) and SDR, especially in the context of Large Eddy Simulations (LES) [40–42]. In this respect, it is worth mentioning that probability density function (PDF) models of scalar mixing requires the expected values of the molecular fluxes conditional upon the scalar value [12] and the micro-mixing term must be modeled; the curvature-related diffusion must be described in terms of calculable statistical moments, or, alternatively, a rigorous criteria to neglect it must be proposed. In addition, the flame curvature affects both the leading edge and flamelet characteristics in statistically steady incompressible turbulent premixed flames [43]. Moreover, curvature contributions can dominate diffusion rates and displacement speed for ignition kernels of small radii [44, 45] and determine their probability of survival. Furthermore, the flame curvature is intrinsically related to the analysis of hydrodynamic and thermos-diffusive instabilities in premixed flames [1–3, 46–48], and the skewness of curvature probability density function can be related to the Darrieus-Landau instability in premixed turbulent flames [48].

From the above discussion, it is evident that flame curvature is a key quantity for the analysis and modelling of turbulent premixed combustion. Therefore, in addition to DNS, several experimental analyses focused on flame curvature statistics. However, almost all experimental measurements of curved combustion fronts employed planar imaging (for example planar laser-induced fluorescence, PLIF), and correspond to 2D curvatures not even in a principal plane of curvature. Shepherd and Ashurst [49, 50] compared planar measurements of curvature and DNS results, showing a reasonable agreement with symmetric PDFs of curvature about zero. Lee et al. [51, 52] obtained PDFs of curvature from OH PLIF, and also show symmetric PDFs of curvature with zero mean value and variance increasing with turbulence intensity. Gashi et al. [53] obtained and compared PDFs of 2D curvatures of turbulent premixed flame kernels with PLIF of OH and 3D curvatures via DNS; the limitations of 2D PLIF curvature measurements are quantified by comparison with the 3D DNS information. Yuen and Gülder [54] investigated premixed methane-air and propane-air turbulent flames stabilized on a Bunsen type burner using planar Rayleigh scattering and PIV; the curvature PDF shows a Gaussian-like behavior at all turbulence intensities for both fuels and at all sections of the flame. Kerl et al. [28] used a quad-plane PIV technique to investigate the 3D behavior of flame displacement speed and front curvature of a premixed methane flame stabilized in a diffuser burner; 2D and 3D data are compared to

critically assess errors of planar measurements. The statistics of 2D curvature PDFs have been compared to 3D curvature PDFs using DNS data [27, 55] and it has been found that 2D statistics compare well with results of planar experimental techniques, but while 2D PDFs are symmetric with nearly zero average mean curvature, 3D PDFs display positive skewness with negative average mean curvature.

Although the aforementioned analyses identified the pivotal role played by curvature in the statistics of displacement speed and SDF, the physical mechanisms responsible for curvature evolution in turbulent premixed flames are yet to be scrutinized in detail. Dopazo et al. [56] derived a transport equation for mean curvature in general Cartesian coordinates and computed the various source terms from a DNS database of mixing inert and reacting fluids at constant density in statistically homogeneous, isotropic turbulence. However, no such analysis has been carried out for turbulent premixed flames, in spite of the pivotal role played by curvature in turbulent premixed flame modelling. This gap is addressed in the present work by analyzing the behavior of the iso-surface curvature transport equation in a turbulent lean methane-air bluff body burner configuration based on a flame-resolved high-fidelity simulation database [57]. The main objectives of this paper are summarized as follows:

- Analysis of the statistics of the various contributions to the curvature evolution equation for a turbulent premixed bluff body burner, which has been analysed in extensive experiments [58–63].
- Identification of the leading order physical mechanisms that contribute to the curvature generation.
- Quantifying the values of the terms in the curvature evolution equation in relation to small-scale flame topologies.

II. MATHEMATICAL BACKGROUND

The transport equation of the reaction progress variable $c(\mathbf{x}, t)$ (which increases monotonically from 0 in fresh reactants to 1 in burnt products) takes the following kinematic form for a given c-isosurface:

$$\frac{\partial c}{\partial t} + v_j^c \frac{\partial c}{\partial x_j} = 0 \tag{1}$$

In this equation, v_j^c is the j^{th} component of the local velocity of a point on the iso-surface element. For the present analysis, the reaction progress variable is defined with the combined mass fractions of CO_2, CO and H_2O ($Y_c = Y_{CO_2} + Y_{CO} + Y_{H_2O}$) in the following manner [37, 57]: $c = [Y_c - Y_c^{min}(\xi)]/[Y_c^{max}(\xi) - Y_c^{min}(\xi)]$, where $Y_c^{max}(\xi)$ and $Y_c^{min}(\xi)$ are the maximum and minimum values of Y_c for a given mixture fraction ξ. The progress variable obeys the transport equation:

$$\frac{\partial c}{\partial t} + v_j \frac{\partial c}{\partial x_j} = \frac{1}{\rho}\frac{\partial}{\partial x_j}\left(\rho D \frac{\partial c}{\partial x_j}\right) + \dot{\omega}_c = \frac{1}{\rho}\frac{\partial}{\partial x_N}\left(\rho D \frac{\partial c}{\partial x_N}\right) + D\frac{\partial c}{\partial x_N} n_{i,i} + \dot{\omega}_c \tag{2}$$

In Eq. (2), v_j is the j^{th} component of the flow velocity, ρ is the fluid density, D is the Fickian molecular diffusivity coefficient for c, and $\dot{\omega}_c$ stands for the production of c by chemical reaction. The local unit vector $\mathbf{n}$ points towards the unburned gas side, normal to the iso-surface, and is defined as: $n_i = -(\partial c/\partial x_i)/|\nabla c| = -c_{,i}/|\nabla c| = c_{,i}/(\partial c/\partial x_N)$, where x_N is the coordinate normal to the iso-surface. Here, $n_{i,i}/2 = 0.5\partial n_i/\partial x_i = 0.5(k_1 + k_2) = k_m$ is the mean value of the two principal curvatures k_1 and k_2 of the iso-surface and will be referred to as the mean flame curvature. The principal curvatures k_1 and k_2 are the eigenvalues of the curvature tensor $\partial n_i/\partial x_j = n_{i,j}$. In particular, the principal curvatures are given by $k_1, k_2 = (-I_1 \pm \sqrt{I_1^2 - 4I_2})/2$ where $I_1 = -\partial n_i/\partial x_i$ and $I_2 = 0.5[(\partial n_i/\partial x_i)(\partial n_j/\partial x_j) - (\partial n_i/\partial x_j)(\partial n_j/\partial x_i)]$ are the first and second invariants of $\partial n_i/\partial x_j$. Based on this convention, the flame surface has a positive (negative) curvature where the flame is convex (concave) to the reactants. The term involving $n_{i,i}$ in Eq. (2) is the molecular diffusion rate tangential to the iso-surface.

Equation (2) can be reformulated for a given c-isosurface [10–20, 22–24, 26, 27, 29, 31, 36] as:

$$\frac{\partial c}{\partial t} + v_j \frac{\partial c}{\partial x_j} = S_d |\nabla c| \tag{3}$$

The local velocity of an iso-surface element is $v_i^c = v_i + S_d n_i$, where S_d is its normal displacement speed relative to the flow. Equating the right sides of Eqs. (2) and (3) yields [10–20, 22–24, 26, 27, 29, 31, 36]:

$$S_d(\mathbf{x},t) = -\frac{1}{\rho(\partial c/\partial x_N)}\frac{\partial}{\partial x_N}\left(\rho D\frac{\partial c}{\partial x_N}\right) - Dn_{j,j} - \frac{\dot{\omega}_c}{(\partial c/\partial x_N)} \tag{4}$$

The displacement speed S_d is the velocity at which the iso-surfaces of the reaction progress variable propagate normal to themselves with respect to an initially coincident material surface. The displacement speed in premixed flames is determined by both reaction and molecular diffusion mechanism, whereas in the passive scalar mixing, the effects of reaction are completely absent. The analysis by Dopazo et al. [56] was done in the context of passive and reactive scalar mixing in a box of constant-density fluid; hence, chemical heat release did not affect the evolution of scalar-gradients and turbulent micro-mixing.

Differentiating Eq. (1) with respect to x_i and setting $c_{,i} = -|\nabla c| n_i$, equations can be obtained for $|\nabla c|$ and n_i [62–64]:

$$\frac{1}{|\nabla c|}\left(\frac{\partial|\nabla c|}{\partial t} + v_j^c\frac{\partial|\nabla c|}{\partial x_j}\right) = -n_i\, v_{j,i}^c\, n_j \tag{5}$$

$$\frac{\partial n_i}{\partial t} + v_j^c\frac{\partial n_i}{\partial x_j} = -\left(\delta_{ij} - n_i n_j\right) S_{jk}^c\, n_k + W_{ij}^c\, n_j \tag{6}$$

In Eqs. (5) and (6), $n_i v_{j,i}^c n_j = n_i S_{ij}^c n_j = a_N^c = a_N + \partial S_d/\partial x_N$ is the total or effective normal strain rate normal to the iso-surface, $a_N = n_i S_{ij} n_j$ is the flow normal strain rate and $\partial S_d/\partial x_N$ is an added normal strain rate induced by molecular mixing and combustion [64–66]. The velocity gradient of a surface element can be expressed as:

$$\begin{aligned} v_{j,i}^c = \frac{\partial v_j^c}{\partial x_i} &= \frac{1}{2}\left(\frac{\partial v_j^c}{\partial x_i} + \frac{\partial v_i^c}{\partial x_j}\right) + \frac{1}{2}\left(\frac{\partial v_j^c}{\partial x_i} - \frac{\partial v_i^c}{\partial x_j}\right) \\ &= \frac{1}{2}\left(\frac{\partial v_j}{\partial x_i} + \frac{\partial v_i}{\partial x_j}\right) + \frac{1}{2}\left(\frac{\partial v_j}{\partial x_i} - \frac{\partial v_i}{\partial x_j}\right) \\ &+ \frac{1}{2}\left(n_j\frac{\partial S_d}{\partial x_i} + n_i\frac{\partial S_d}{\partial x_j}\right) + \frac{1}{2}\left(n_j\frac{\partial S_d}{\partial x_i} - n_i\frac{\partial S_d}{\partial x_j}\right) \\ &+ S_d\frac{1}{2}\left(\frac{\partial n_j}{\partial x_i} + \frac{\partial n_i}{\partial x_j}\right) + S_d\frac{1}{2}\left(\frac{\partial n_j}{\partial x_i} - \frac{\partial n_i}{\partial x_j}\right) \end{aligned} \tag{7}$$

The nomenclature associated with terms on the right side of Eq. (7) is summarized in Table I, where the total strain rate and rotation rate tensors are expressed as $S_{ij}^c = S_{ij} + S_{ij}^a$ and $W_{ij}^c = W_{ij} + W_{ij}^a$, respectively [64–66].

TABLE I: Nomenclature associated with the velocity gradient $v_{i,j}^c$ of an iso-surface element.

Description	**Term**
Total strain rate tensor	$S_{ij}^c = 0.5(\partial v_i^c/\partial x_j + \partial v_j^c/\partial x_i)$
Total rotation rate tensor	$W_{ij}^c = 0.5(\partial v_i^c/\partial x_j - \partial v_j^c/\partial x_i)$
Flow strain rate tensor	$S_{ij} = 0.5(\partial v_i/\partial x_j + \partial v_j/\partial x_i)$
Flow rotation rate tensor	$W_{ji} = 0.5(\partial v_i/\partial x_j - \partial v_j/\partial x_i)$
Added strain rate tensor	$S_{ij}^a = \underbrace{0.5[(\partial S_d/\partial x_j)n_i + (\partial S_d/\partial x_i)n_j]}_{\textit{Space dependence of } S_d} + \underbrace{S_d 0.5(\partial n_i/\partial x_j + \partial n_j/\partial x_i)}_{\textit{Propagating curved iso-c}}$
Added rotation rate tensor	$W_{ij}^a = \underbrace{0.5[(\partial S_d/\partial x_j)n_i - (\partial S_d/\partial x_i)n_j]}_{\textit{Space dependence of } S_d} + \underbrace{S_d 0.5(\partial n_i/\partial x_j - \partial n_j/\partial x_i)}_{\textit{Propagating curved iso-c}}$

TABLE II: Description of the various terms in the mean curvature transport equation (8).

Terms	**Description**	**Terms**	**Description**
T_1	Contribution due to curvature/flow normal strain rate	T_6	Contribution due to curvature/added normal strain rate
T_2	Contribution due to flow normal strain rate normal variation	T_7	Contribution due to added normal strain rate normal variation
T_3	Curvature flow stretching term	T_8	Curvature added flow stretching term
T_4	Contribution due to flow strain rate gradients	T_9	Contribution due to added strain rate gradients
T_5	Contribution due to flow vorticity curl	T_{10}	Contribution due to added vorticity curl

The flow strain rate and rotation rate tensors S_{ij} and W_{ij} are due to the fluid motion, and the added strain rate and rotation rate tensors S_{ij}^a and W_{ij}^a are due to the motion of curved iso-surfaces relative to the flow with spatially dependent S_d. The first term on the right side of Eq. (6) for n_i is the projection of the strain vector $-\mathbf{S}^c \cdot \mathbf{n}$ on a plane perpendicular to $\mathbf{n}$, whereas the second term $W_{ij}^c n_j = \frac{1}{2}\varepsilon_{ijk}\omega_j^c n_k$ is the solid body rotation of $\mathbf{n}$ with an angular velocity $\frac{1}{2}\boldsymbol{\omega}^c$ (the total vorticity vector $\boldsymbol{\omega}^c = \nabla \times \mathbf{v}^c = \nabla \times \mathbf{v} + \nabla \times (S_d\mathbf{n})$ at a point on the iso-surface is the sum of the flow vorticity $\boldsymbol{\omega} = \nabla \times \mathbf{v}$ and the added vorticity $\boldsymbol{\omega}^a = \nabla \times (S_d\mathbf{n}) = \nabla S_d \times \mathbf{n} + S_d \nabla \times \mathbf{n}$). Both contributions are perpendicular to $\mathbf{n}$ [56].

Taking the derivative of Eq. (6) for n_i with respect to x_i yields an evolution equation for the mean curvature k_m [56]:

$$\frac{\partial k_m}{\partial t} + v_j^c \frac{\partial k_m}{\partial x_j} = \underbrace{\underbrace{\frac{a_N n_{i,i}}{2}}_{T_1} + \underbrace{\frac{1}{2}\frac{\partial a_N}{\partial x_N}}_{T_2} \underbrace{-S_{ij} n_{j,i}}_{T_3} \underbrace{-\frac{1}{2}\frac{\partial S_{ij}}{\partial x_i} n_j}_{T_4} + \underbrace{\frac{1}{2}\frac{\partial W_{ij}}{\partial x_i} n_j}_{T_5}}_{flow\ terms} + \underbrace{\underbrace{\frac{1}{2}\frac{\partial S_d}{\partial x_N} n_{i,i}}_{T_6} + \underbrace{\frac{1}{2}\frac{\partial^2 S_d}{\partial {x_N}^2}}_{T_7} \underbrace{-S_{ij}^a n_{j,i}}_{T_8} \underbrace{-\frac{1}{2}\frac{\partial S_{ij}^a}{\partial x_i} n_j}_{T_9} + \underbrace{\frac{1}{2}\frac{\partial W_{ij}^a}{\partial x_i} n_j}_{T_{10}}}_{added\ terms} \quad (8)$$

The right hand side of Eq. (8) shows: *i*) the terms T_{1-5} arising from the fluid flow, and *ii*) the terms T_{6-10} added by molecular mixing and combustion. Positive terms on the right side of Eq. (8) are sources of mean curvature and tend to increase the convexity of iso-surfaces; negative terms are sinks that decrease the convexity. The physical meaning of the terms in Eq. (8) is summarized in Table II.

The terms T_5 and T_{10} in Eq. (8) can be recast as [56]:

$$T_5 = \frac{1}{2}\frac{\partial W_{ij}}{\partial x_i} n_j = \frac{1}{4} n_i \varepsilon_{ijk} \frac{\partial \omega_k}{\partial x_j} \quad (9)$$

$$T_{10} = \frac{1}{2}\frac{\partial W_{ij}^a}{\partial x_i} n_j = \frac{1}{4} n_i \varepsilon_{ijk} \frac{\partial \omega_k^a}{\partial x_j} = -\frac{1}{4}(\delta_{ij} - n_i n_j)\frac{\partial^2 S_d}{\partial x_i \partial x_j} + \frac{1}{4}\left(\frac{\partial S_d}{\partial x_N}\frac{\partial n_j}{\partial x_j} + \frac{\partial S_d}{\partial x_j}\frac{\partial n_j}{\partial x_N}\right) - \frac{1}{4} S_d n_i \frac{\partial}{\partial x_j}\left(\frac{\partial n_i}{\partial x_j} - \frac{\partial n_j}{\partial x_i}\right) \quad (10)$$

Results for the terms T_{1-10} are presented after normalisation $T_\alpha^* = T_\alpha(\delta_L^2/S_L)$ and conditioned on small-scale flame geometries later in this paper. These local iso-scalar geometries can be characterized in terms of the mean curvature $k_m = 0.5(k_1 + k_2)$ and the Gauss curvature $k_g = k_1 k_2$, as shown in Fig. 1 [67]. The region of complex curvatures cannot be realized in practice. The small-scale geometries associated with $k_g > 0$ correspond to cup-convex and cup-concave structures for $k_m > 0$ and $k_m < 0$ respectively. The structures with $k_g < 0$ lead to saddle-like geometries, which can be either positively (i.e. $k_m > 0$) or negatively (i.e. $k_m < 0$) curved. A zero value of k_g leads to tile structures, either tile convex or tile concave for $k_m > 0$ or $k_m < 0$. Figure 1 will subsequently be used in this paper to facilitate the

discussion related to the iso-surface geometries in the $k_m - k_g$ plane [67]. The results are presented in normalized form, for $k_m^* = k_m \delta_L$ and $k_m^* = k_m \delta_L^2$, where δ_L is the laminar flame thickness $\delta_L = (T_{ad} - T_u)/\max|\nabla T|_L$. The subindex L refers to unstrained laminar flame values.

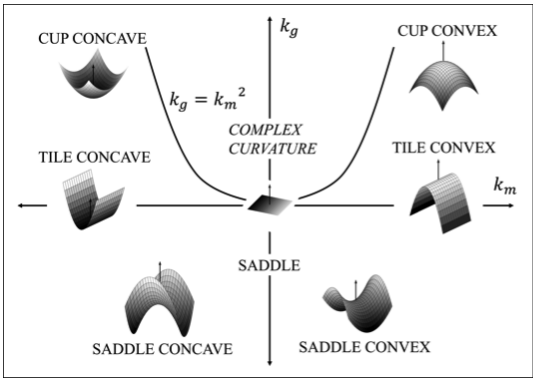

FIG. 1: Classification of iso-surface geometries in the plane of mean k_m and Gauss curvature k_g [67].

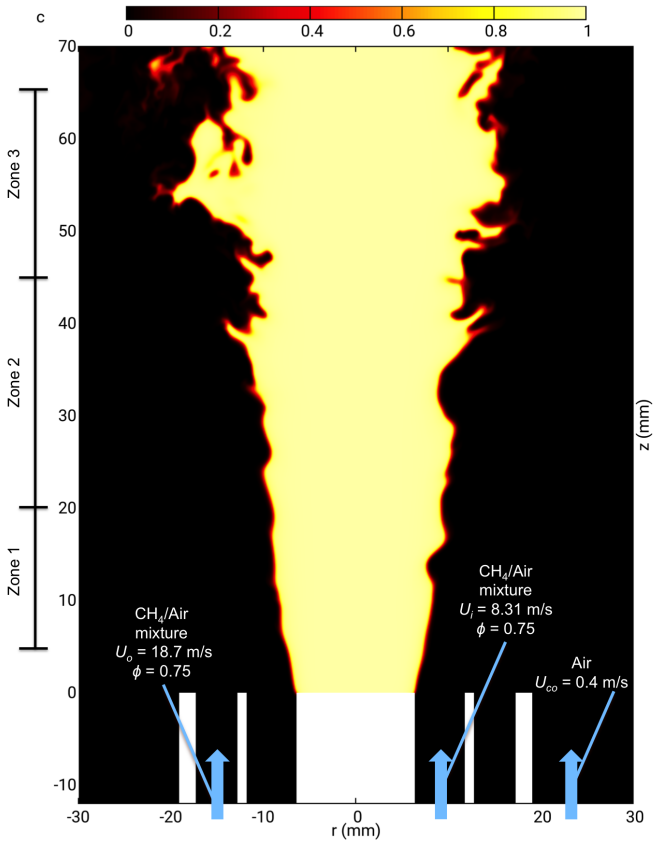

FIG. 2: Instantaneous progress variable c in the burner mid section.

III. NUMERICAL IMPLEMENTATION

The flame resolved simulation has been described by Sandeep et al. [37] and Proch et al. [57] in detail, and only a brief summary is provided here. The Cambridge stratified flame has been simulated by various groups applying RANS, LES [68–70] and the highly resolved simulation of the present case. Experimental data was provided by Hochgreb and Barlow and co-workers [58–63], leading to the unique situation that 'flame DNS' data could be validated against a real flame experiment.

The burner consists of a bluff body surrounded by two co-annular methane-air streams with an equivalence ratio of $\phi = 0.75$ at atmospheric conditions, embedded in an air-coflow with a velocity of 0.4 m/s, as illustrated in Fig. 2. The Lewis number was unity for all species and the chemistry was tabulated with the Premixed Flamelet Generated Manifolds (PFGM) approach [71–73]. The Kolmogorov micro-scale is η=41 μm at the inlet and increases significantly downstream and from the unburned to the burned side of the flame. The ratio of the grid resolution to the Kolmogorov micro-scale in the reaction zone is $\Delta/\eta \approx 1$, which means that the velocities scales are resolved. Results are analyzed at $t = 0.34$ s, many initial integral eddy turnover times ($\tau = 60 \times 10^{-5}$ s based on the inner stream mean velocity) into the simulation and after one flow-through time ($t = 0.28$ s) of the slow air co-flow. Table III gives the inlet flow velocities of the co-annular streams U, the integral length scale l, the root-mean-square turbulent velocity fluctuation u', the unstrained laminar burning velocity S_L, the Damköhler number $Da = lS_L/u'\delta_L$, Karlovitz number $Ka = (u'/S_L)^{3/2}(l/\delta_L)^{-1/2}$, and turbulent Reynolds number $Re_t = u'l/\nu$ where the kinematic viscosity ν depends on the temperature. The statistics have been evaluated at different axial locations above the burner, namely, in Zone 1 (5-20 mm), Zone 2 (20-45 mm) and Zone 3 (45-65 mm) as illustrated in Fig. 2. The value of u'/S_L increases, whereas l/δ_L does not change appreciably with increasing axial distance [57]. This suggests that $Ka = (u'/S_L)^{3/2}(l/\delta_L)^{-1/2}$ increases in the downstream direction and combustion takes place at the boundary of the corrugated flamelets and thin reaction zones regimes of combustion [74] close to the inlet, whereas combustion takes place well within the thin reaction zones regime away from the nozzle inlet. Interested readers are referred to Fig. 15 of Ref. [57] for further information in this regard.

TABLE III: Parameters of the inner and outer reactants streams.

Stream	l	u'	S_L	δ_L	Re	ϕ	Da	Ka	Re_t
	mm	m/s	m/s	mm	-	-	-	-	-
Inner	0.5	0.9	0.21	0.56	5,960	0.75	0.2	9.3	28.1
Outer	0.5	1.8	0.21	0.56	11,500	0.75	0.1	26.3	56.3
$U_i = 8.31$ m/s, $U_0 = 18.7$ m/s and $U_{co} = 0.4$ m/s									

IV. RESULTS AND DISCUSSIONS

A. Terms of the curvature evolution equation conditional upon the progress variable

Figure 3 shows the mean values of the terms in the curvature transport equation (8), conditioned on the reaction progress variable c for the three axial locations (Zone 1: 5-20 mm, Zone 2: 20-45 mm, Zone 3: 45-65 mm). The ensemble averages were extracted from the given iso-surfaces at $t = 0.34$ s, as in previous analyses [16–20, 55, 75]. The flame width changes significantly in the axial direction (see Figs. 9 and 19 of Proch et al. [57]) and thus plotting the terms conditional on c is more sensible for the purpose of comparison of the curvature transport terms between different zones. It is apparent that some of the added terms arising from flame propagation (see Table II) are one or two orders of magnitude greater than most flow contributions, depending on the axial location in the flame, as illustrated in Fig. 3(c).

The mean values of the flow terms T_{1-5} conditioned on c increase with the axial height as the flame wrinkling increases downstream. Terms T_2, T_3 and T_4 seem to be the dominant. The mean value of the term due to curvature and flow normal strain rate, $T_1^* = T_1(\delta_L^2/S_L) = [(a_N n_{i,i})/2](\delta_L^2/S_L)$, assumes weak positive values for $c > 0.3$ near the burner and becomes increasingly negative downstream; the latter implies that $a_N > 0$ is predominantly associated with concave local structures ($k_m < 0$), while $a_N < 0$ occurs for convex topologies ($k_m > 0$). It has been demonstrated earlier that flame wrinkling increases further away from the burner where some turbulent eddies penetrate the preheat region, thereby increasing the magnitude of curvature $k_m = n_{i,i}/2$. The turbulent straining dominates over the flame normal acceleration [15, 31], as the axial distance from the burner increases, which gives rise to a preferential alignment of ∇c with the eigenvector associated with the most compressive principal strain rate [37, 57, 76]. Thus, the share of negative

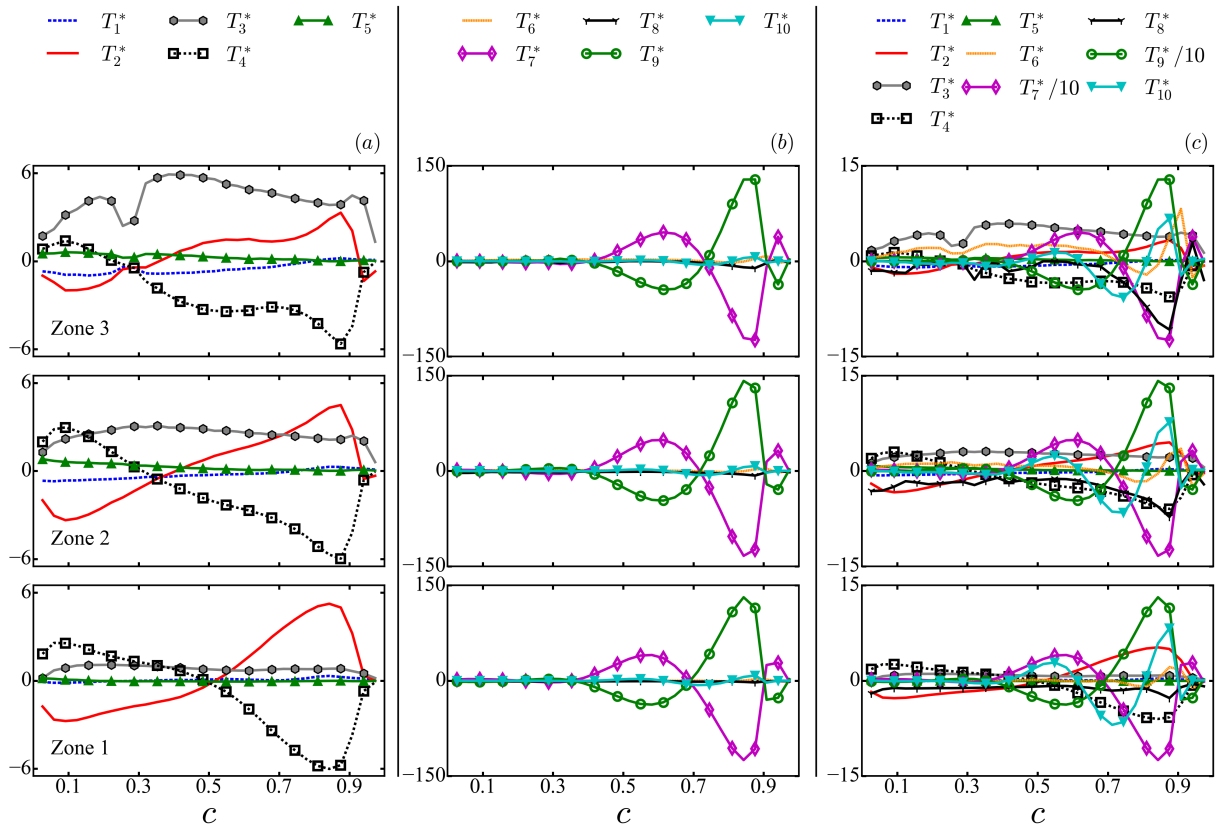

FIG. 3: Average values of the mean curvature transport terms of Eq. (8), conditioned on the reaction progress variable c at different axial locations. (a) Flow terms; (b) added terms; (c) all terms, the mean values of T_7^* and T_9^* have been scaled by ten. Results are separately examined in three zones (Zone 1: 5-20 mm, Zone 2: 20-45 mm, Zone 3: 45-65 mm).

values of a_N increases downstream (not shown here) [37], and the negative values of a_N are more frequent for convex ($k_m > 0$) flame topologies [77]. Furthermore, the effects of dilatation are strong in the negatively curved regions [17, 18, 26, 37] because of the focusing of heat, and this increases the extent of ∇c alignment with the most extensive principal strain rate, which produces locally either positive or small negative values of a_N. The negative correlation between a_N and k_m [37] leads to the negative mean values of T_1^* away from the nozzle exit.

The mean values of $T_2^* = T_2(\delta_L^2/S_L) = [(\partial a_N/\partial x_N)/2](\delta_L^2/S_L)$, which is due to the normal gradients of the flow normal strain rate, assumes negative values on the unburnt side, shifting towards positive values in the reaction layer and retains this behaviour in different zones above the burner exit. This is consistent with the dependence of a_N on x_N in this flame [37, 57]; a_N increases from the fresh reactants ($\partial a_N/\partial x_N < 0$), reaches

a maximum within the flame and decreases towards the hot products ($\partial a_N/\partial x_N > 0$). Thermal expansion due to heat release within the reaction zone promotes the alignment of ∇c with the most extensive principal strain rate, and yields a maximum of a_N in the reaction zone.

The mean value of the curvature flow stretching term $T_3^* = T_3(\delta_L^2/S_L) = -(S_{ij}n_{j,i})(\delta_L^2/S_L)$ assumes mostly positive values, with a significant increase in magnitude in the downstream direction. Using the principal axes tangent to a local iso-surface ($\mathrm{x}_{T1}, \mathrm{x}_{T2}$), the curvature flow stretching term can be written as $T_3 = -(S_{11}k_1 + S_{22}k_2)$, where S_{11} and S_{22} are the unitary tangential strain rates along axes x_{T1} and x_{T2}, respectively, and k_1 and k_2 are the principal curvatures. It is worth noting that $a_T = S_{11} + S_{22}$ and a_N may predominantly assume positive values when ∇c predominantly aligns with the eigenvector associated with the most extensive principal strain rate [37, 57, 76]. A positive value of T_3 implies a combination of elliptic and hyperbolic scalar topologies [67] with positive and negative values of k_1 and k_2. For example, an elliptic concave structure ($k_1 < 0$ and $k_2 < 0$), yields $T_3 > 0$ for a combination of $S_{11} > 0$ and $S_{22} > 0$.

The profile of the mean value of the term $T_4^* = -[(\partial S_{ij}/\partial x_i)(n_j/2)](\delta_L^2/S_L)$ conditional upon c is similar to that of $-T_2^*$. This means that the two vectors n_j and $\partial S_{ij}/\partial x_i$ point in the same direction within the flame, but tend to point in opposite directions on the unburned side of the flame.

The mean contribution to the curvature evolution due to vorticity gradients, $T_5^* = T_5(\delta_L^2/S_L) = [(\partial W_{ij}/\partial x_i)(n_j/2)](\delta_L^2/S_L)$, can be rewritten as $T_5^* = \{(n_i/4)[\varepsilon_{ijk}(\partial\omega_k/\partial x_j)]\}(\delta_L^2/S_L)$, in vector notation $T_5 = [\mathbf{n}\cdot(\nabla\times\boldsymbol{\omega})]/4$ (see Eq. (9)). For example, on an iso-surface and using the local principal axes ($\mathrm{x}_{T1}, \mathrm{x}_{T2}, \mathrm{x}_{N3}$), T_5 can be expressed as $T_5 = (\partial\omega_2/\partial x_1 - \partial\omega_1/\partial x_2)/4$ for $\mathbf{n} = (0, 0, 1)$, where ω_1 and ω_2 are components of the flow vorticity vector tangent to the c iso-surface. It can readily be seen that co-rotating parallel vortices of different intensity and counter-rotating parallel vortices of the same intensity can curve a planar local iso-surface structure, fostering positive or negative curvatures. The mean value of T_5 shifts from small negative values close to the burner to positive values further downstream. The flame-turbulence interaction is weak in Zone 1 [37, 57], but some vortical structures penetrate the preheat region in Zones 2 and 3, which increases the spatial variation of vorticity, in turn increasing the magnitude of T_5 towards the unburned gas side and in the downstream direction. The mean contribution by vorticity gradients T_5^* remains

mostly negligible close to $c = 1.0$ due to the annihilation of enstrophy by dilatation and the high dynamic viscosity in the hot products.

The mean values of the added terms due to flame propagation T_6^*, T_8^* and T_{10}^* have negligible values in comparison to those of the terms T_7^* and T_9^* through most of the flame brush. The mean contributions of T_7^* and T_8^* exhibit similar trends towards the burned gas side of the flame in Zones 2 and 3 (see Fig. 3(c)). High values of $k_m = n_{i,i}/2$ are less probable to occur in Zone 1 since the flame propagates in a low turbulence environment. This behaviour explains the small mean contributions to the curvature evolution in Zone 1 due to the source term of curvature and added normal strain rate $T_6^* = [(\partial S_d/\partial x_N)(n_{i,i}/2)](\delta_L^2/S_L)$, and due to the added flow stretching term $T_8^* = -(S_{ij}^a n_{j,i})(\delta_L^2/S_L)$. The term T_6^* is associated with scalar topologies corresponding to compressive and extensive added normal strain rates.

The term $T_7^* = T_7(\delta_L^2/S_L) = [(\partial^2 S_d/\partial x_N^2)/2](\delta_L^2/S_L)$ results from the flame normal gradient of the added normal strain rate. The mean variation of $\partial S_d/\partial x_N$ conditioned upon c has been shown for this case before [37] and is not repeated here. In the present case, the mean value of $\partial S_d/\partial x_N$ assumes predominantly negative values for the major part of the flame front before assuming weak positive values on the burned gas side. By contrast, in Zones 2 and 3, the mean value of $\partial S_d/\partial x_N$ remains positive on both unburned gas and burned gas sides of the flame front and negative values are only obtained in the reaction zone (i.e. $0.6 < c < 0.9$). Accordingly, the mean values of T_7^* are monotonically increasing from the unburned gas side towards the preheat region taking negative values in the region with high chemical activity, and positive on the burned gas side; T_7^* changes sign from the leading edge to the preheat/burning region to the trailing edge of the flame.

The mean contribution to the added stretching term, $T_8^* = T_8(\delta_L^2/S_L) = -(S_{ij}^a n_{j,i})(\delta_L^2/S_L)$, exhibits small magnitudes in Zone 1, since high values of $n_{i,i}$ are less probable to occur in Zone 1 where the flame propagates in a low turbulence environment. The mean values of T_8^*, conditional on c, increase in the downstream direction and attain significant peak values in the reaction zone of the flame. For example, on an iso-surface and using the local principal axes $(\mathrm{x}_{T1}, \mathrm{x}_{T2}, \mathrm{x}_{N3})$, T_8 takes the form $T_8 = -S_d(k_1^2 + k_2^2)$, for $\mathbf{n} = (0, 0, 1)$, which accordingly yields a negative value in the reaction zone.

The mean contribution due to the added strain gradients $T_9^* = T_9(\delta_L^2/S_L) = -[(\partial S_{ij}^a/\partial x_i)(n_j/2)](\delta_L^2/S_L)$ depends on the second derivatives of S_d and of n_i, and on cross products of the gradients of S_d and the curvature tensor; the profile of the mean value of this

term conditional upon c is similar to that of $-T_7^*$. The mean value of the added vorticity curl contribution $T_{10}^* = T_{10}(\delta_L^2/S_L)$ exhibits a small magnitude in Zone 1 and increases in downstream direction with significant positive peak values in the reaction zone of the flame of this flow configuration.

B. Terms of the curvature evolution equation conditional upon the flame curvature

The mean flow contributions T_{1-5}^* and the added contributions T_{6-10}^* to the mean curvature evolution conditioned upon the normalised mean curvature $k_m^* = k_m\delta_L$ are shown in Fig. 4. It can be seen that the added contributions dominate over the flow contributions for all values of k_m^*, which agrees with the results observed in Fig. 3. No clear trend exists between k_m^* and the flow terms in Zone 1. The flow does not influence small-scale scalar structures in this zone due to weak flame-turbulence interaction. In Zones 2 and 3, negative values of $T_1^* = T_1(\delta_L^2/S_L) = [(a_N n_{i,i})/2](\delta_L^2/S_L)$ are related to $k_m^* < 0$, whereas $T_1^* > 0$ correspond to $k_m^* > 0$; it is worth stressing that different iso-surfaces are analyzed in these averages, and since the flow normal strain rate a_N is predominantly negative downstream [37], the variation of T_1^* is determined by the mean curvature $k_m = n_{i,i}/2$. On the other hand, T_2^* seems to be approximately constant for every scalar geometry since there is no correlation between T_2^* and k_m^*. The term $T_3^* = T_3(\delta_L^2/S_L) = -(S_{ij}n_{j,i})(\delta_L^2/S_L)$ acts as the leading flow term for topologies with large curvatures, both concave and convex. The profiles of T_4^* and T_5^* across the mean curvature are similar. These terms have negligible values towards negative k_m for increasing positive values of mean curvature, indicating that gradients of flow strain and rotation rates tend to align with the normal vector $\mathbf{n}$ for convex scalar micro-structures.

The mean values conditioned on curvature for T_6^* and T_7^* remain negligible across the flame-front in every zone. The curvature added stretching term $T_8^* = T_8(\delta_L^2/S_L)$ exhibits a positive correlation with k_m; it has already been mentioned in Section IV A that an approximation in principal axes of curvature yields $T_8 = -S_d(k_1^2 + k_2^2)$, which implies a cubic dependence on k_m accounting for the dependency of S_d on mean curvature; so that T_8 shows an antisymmetric behavior with respect to $k_m = 0$, with its negative values correlating with $k_m < 0$, and positive values corresponding to $k_m > 0$; $k_m = 0$ being the inflection

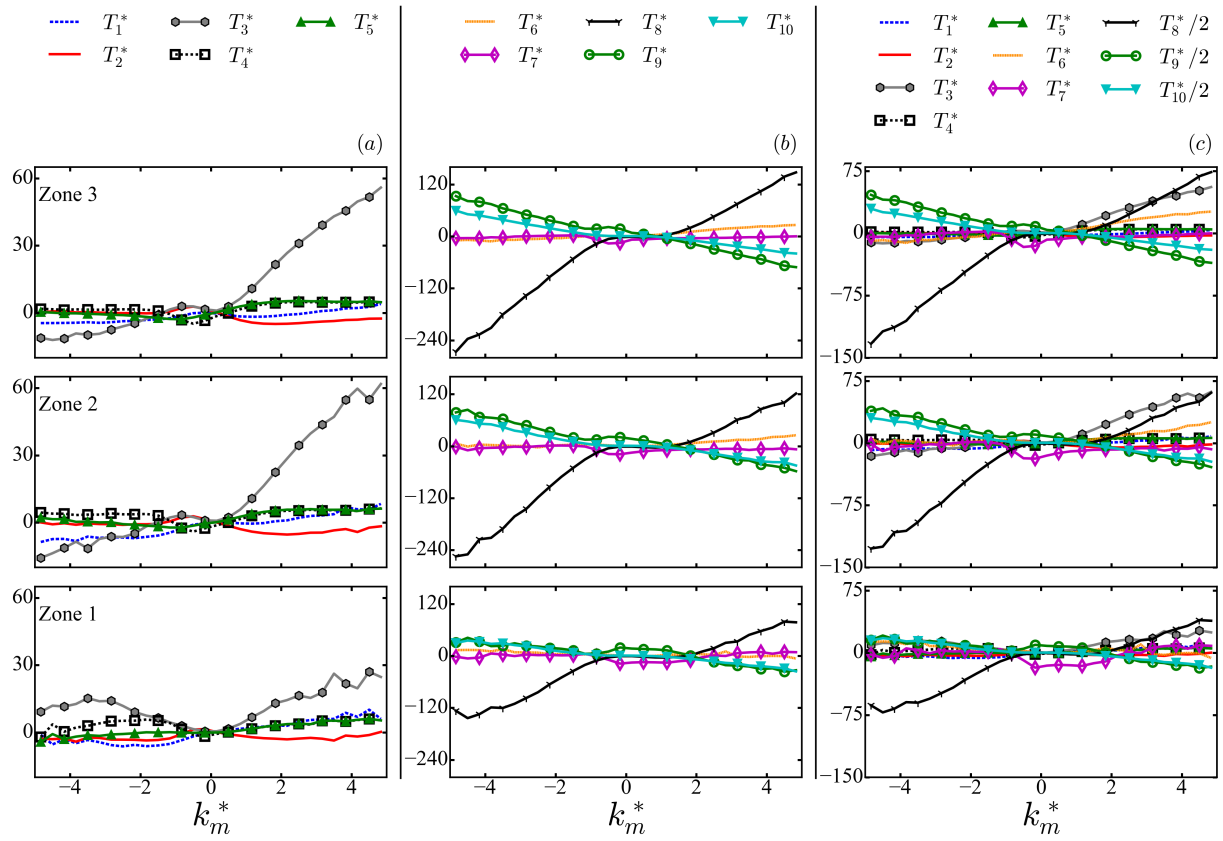

FIG. 4: Average values of the mean terms in the curvature transport equation (8), conditioned upon the mean curvature k_m^*. (a) Flow terms; (b) added terms; (c) all terms, the mean values of T_8^*, T_9^* and T_{10}^* have been scaled by two. Results are separately examined in three zones (Zone 1: 5-20 mm, Zone 2: 20-45 mm, Zone 3: 45-65 mm).

point. The mean contribution due to the added strain gradients T_9^* and the mean value of the added vorticity curl contribution T_{10}^* display negative correlations with k_m, which indicates that the significant positive values correlated with the reaction zone of the flame are mainly associated to concave iso-scalar surfaces; these negative correlations are also observed in previous studies between the local volumetric dilatation rate and the mean flame curvature [17, 78].

C. Flow, added and total contributions to the curvature evolution

The mean values of flow contributions ($T_1^* + \ldots + T_5^*$), the flame propagation induced added contributions ($T_6^* + \ldots + T_{10}^*$) and the total contribution ($T_1^* + \ldots + T_{10}^*$) to the curvature evolution, conditioned on the reaction progress variable c and the mean curvature k_m^*, for the different zones of the computational domain are shown in Fig. 5.

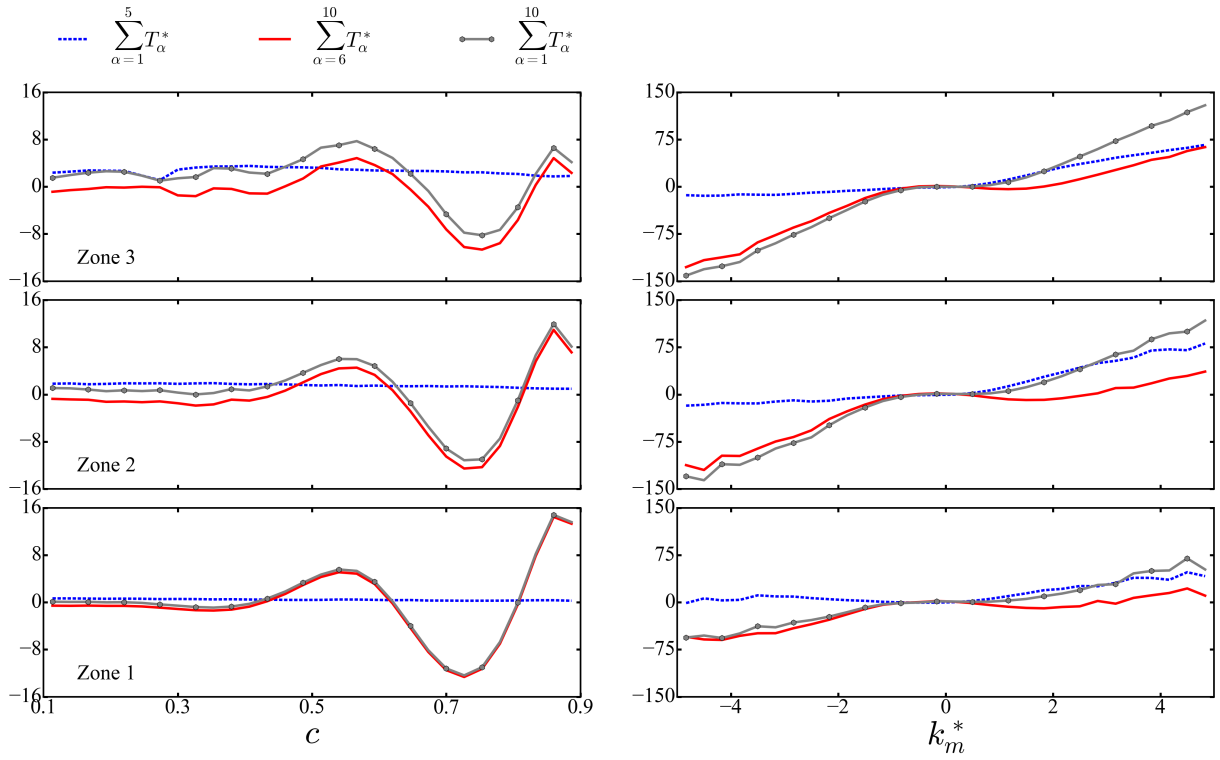

FIG. 5: Contribution of flow and added source terms and sum of all the terms, conditioned on the reaction progress variable c and the mean curvature k_m^*. Results are separately examined in three zones (Zone 1: 5-20 mm, Zone 2: 20-45 mm, Zone 3: 45-65 mm).

The overall contributions conditioned on c are positive (convexity increases, concavity decreases) in the unburned gas and the preheat regions, and become negative (convexity decreases, concavity increases) in the reaction zone of the flame with positive values in the burnt products. This implies that the positive mean contributions of T_3^* and T_4^* dominate over the flame propagation induced added contributions in the unburned gases. On the contrary, T_7^* is the leading term in the reaction zones and in the burned gas side of the flame front. The total contribution to the k_m evolution is controlled by flow terms on the unburned gas side (i.e. $c < 0.5$), and by the flame propagation-induced added terms for $c > 0.5$. The mean overall flow contribution conditioned on k_m^* is negligible in comparison with the overall added contribution for negative values of k_m^*, but assumes non-negligible values for $k_m^* > 0$. Added flow terms are negligible compared with the flow terms for $k_m^* > 0$ in Zone 1. In Zones 2 and 3, the magnitude of the flow terms increases for $k_m^* > 0$. It can also be seen that the overall mean added contribution arises mainly from the term T_8^*, due to curvature added flow stretching.

D. Terms of the curvature evolution equation conditional upon the local geometry of iso-scalar surfaces

To analyze the small-scale structures and local topologies, the joint probability density functions (JPDF) of the mean and Gauss curvatures k_m^* and k_g^* for three regions, namely unburned gases ($c = 0 - 0.1$), flame ($c = 0.1 - 0.9$) and hot products ($c = 0.9 - 0.99$), are shown in Fig. 6. It can be seen from Fig. 6 that the ranges of k_m^* and k_g^* broaden from Zone 1 to Zone 3 as the flame becomes increasingly wrinkled in downstream direction [37, 57]. The JPDFs are presented in the various zones above the burner exit in order to identify the effects of the flame-turbulence interaction in the downstream direction. The regions unburned and products do not show a significant chemical activity (as expected), whereas a large positive dilation rate is found in the flame region due to heat release [37, 57]. It can be seen that nearly flat iso-scalar surfaces are the most probable geometries in all zones. Flat structures are evident very close to the burner exit where the flame wrinkling is weak. In the unburned gases, the JPDF appears to be symmetrical about $k_m^* = 0$ and this behavior does not change with the axial distance. In the flame region, the JPDF is slightly skewed towards positive values of k_m^*, reflecting the features of evolving small-scale structures due to turbulence in the zone of intense chemical activity. This behavior is prominent in Zone 3, where flame wrinkling increases due to turbulence effects. Towards the products region, the probability of finding concave scalar structures decreases drastically and nearly flat or convex geometries are most probable; this behavior can be attributed to the focusing of heat by concave geometries. Convex iso-surfaces with moderate k_m^* values, particularly the convex elliptical cup geometries, survive in the products region.

Figure 7 shows the mean values of the flow contributions T_{1-5}^* to the generation/annihilation of mean curvature conditional upon the mean k_m^* and Gauss k_g^* curvatures. The mean values of the added contributions T_{6-10}^* conditional upon k_m^* and k_g^* are shown in Fig. 8. Moderate and large positive values of the different terms, especially the major contributors T_3 and T_8, correlate with $k_m^* > 0$, with iso-scalar surface geometries of a convex-elliptic nature, whereas the negative values of these terms are associated with flat and concave geometries. These trends are in agreement with the observed results from Fig. 5, and also suggest that the negative (positive) values of the curvature transport equation correspond to concave (convex) scalar micro-structures. On the other hand, the main

added contributions T_9 and T_{10} display negative correlations with k_m similar to those found in previous studies between the local volumetric dilatation rate and the mean flame curvature [17, 78], where large positive dilatation rate values are obtained due to focussing of heat at concave geometries.

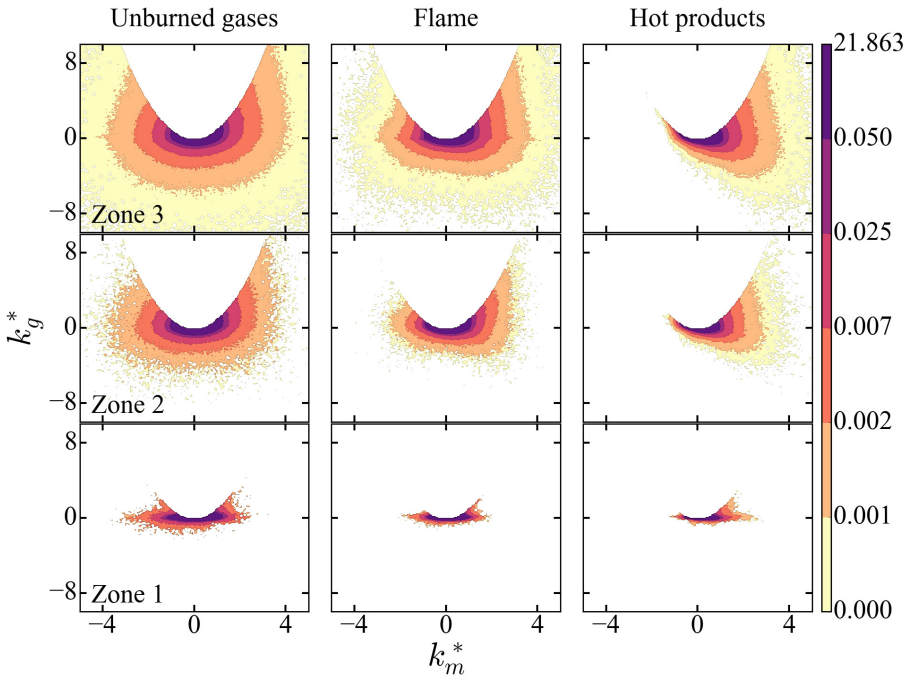

FIG. 6: JPDFs of the mean curvature k_m^* and Gauss curvature k_g^*. Results are separately examined in three zones (Zone 1: 5-20 mm, Zone 2: 20-45 mm, Zone 3: 45-65 mm), and in three regions, namely unburned gases ($c = 0 - 0.1$), flame ($c = 0.1 - 0.9$) and hot products ($c = 0.9 - 0.99$).

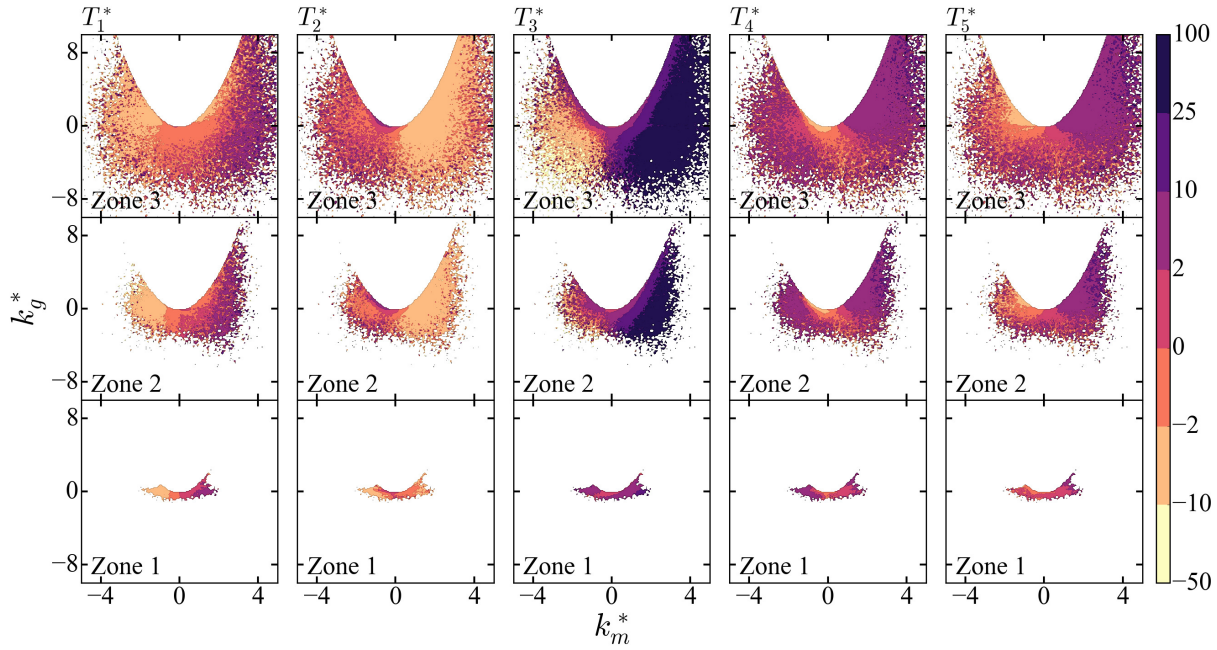

FIG. 7: Conditional mean of flow terms upon the mean curvature k_m^* and Gauss curvature k_g^* in the flame region ($c = 0.1 - 0.9$). Results are separately examined in three zones (Zone 1: 5-20 mm, Zone 2: 20-45 mm, Zone 3: 45-65 mm).

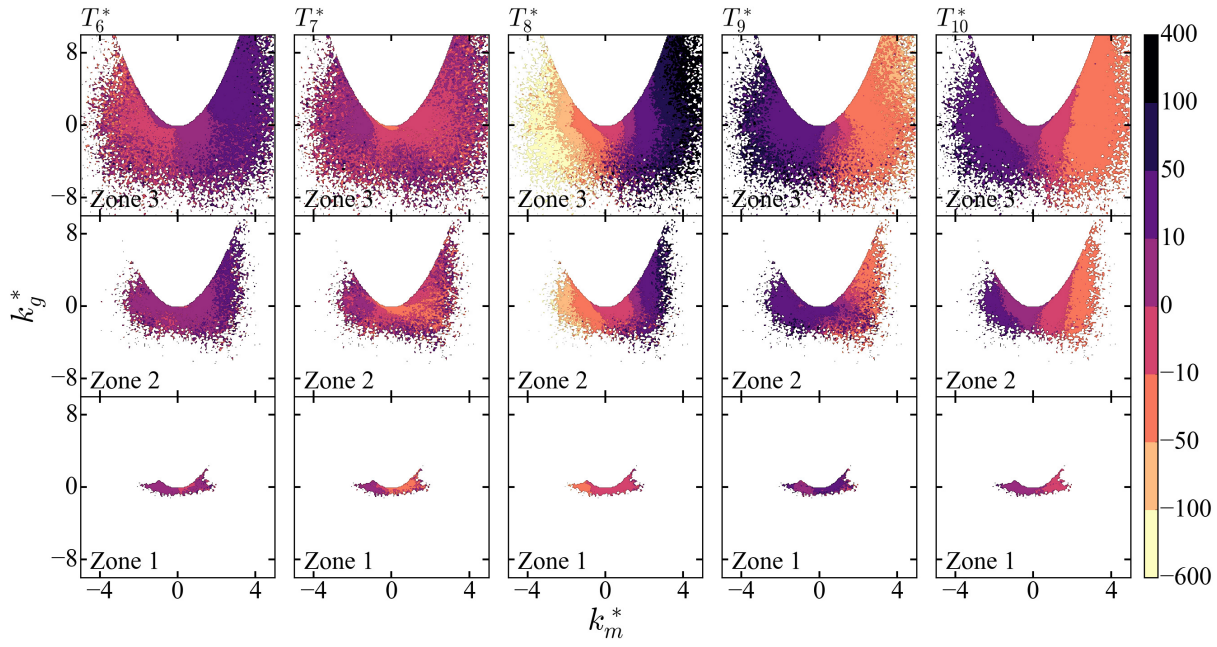

FIG. 8: Conditional mean of added terms upon the mean curvature k_m^* and Gauss curvature k_g^* in the flame region ($c = 0.1 - 0.9$). Results are separately examined in three zones (Zone 1: 5-20 mm, Zone 2: 20-45 mm, Zone 3: 45-65 mm).

E. Implications of the results

The findings based on Figs. 3 to 5 and 7 reveal that the added contributions to the curvature k_m arising from displacement speed S_d play the dominant role in the reaction zone and the burned gas side of the flame front. This essentially indicates that curvature and displacement speed are intrinsically interlinked. Therefore, curvature not only affects the local displacement speed (a dominant negative correlation between S_d and k_m exists in this flame at all locations [37, 57]), as this displacement governs the curvature evolution and thus flame wrinkling in turn. Moreover, the flow contribution arising from the flow stretching term $T_3 = -2(S_{ij}n_{j,i})$ and the contribution due to flow strain rate gradients $T_4 = -(\partial S_{ij}/\partial x_i)(n_j/2)$ are found to govern flame curvature evolution on the unburned gas side, where the reaction effects are not strong. As both curvature and displacement speed have significant influences on the evolution of $|\nabla c|$ [18, 23, 35–37], they have implications on FSD and SDR evolutions [40–42] and thus on the closure of molecular mixing and micro-mixing in PDF methods [65, 79]. Thus, it is not surprising that the normal strain rate and displacement speed play key roles in the evolutions of curvature, SDF, FSD and SDR. Furthermore, some of the behaviours of the instantaneous curvature transport equation will be visible for the resolved curvature in the context of Large Eddy Simulations (LES), so that the statistics of the displacement speed and flame normal strain rate (in other words scalar gradient alignment with local principal strain rates) need to be adequately accounted for to accurately predict the resolved flame wrinkling. However, this necessity is not limited to the resolved scale, and the aforementioned physical mechanisms determine sub-grid scale wrinkling and influence the closure of sub-grid terms related to curvature in both the FSD and SDR transport equations [40–42].

V. CONCLUSIONS

Flame resolved high-fidelity simulation data of a turbulent premixed bluff body burner has been used to examine the evolution of mean curvature. This involves the terms arising from the fluid flow and from the non-material nature of the propagating flame iso-surfaces. It has been shown that the contributions to the curvature evolution equation due to the fluid flow play an important role on the unburned gas side, whereas the added terms due to flame

propagation dominate the reaction region and in the hot products. The curvature added flow stretching term $T_8 = -2(S^a_{ij} n_{j,i})$, which is a combination of the curvature tensor and gradients of flow and diffusion/chemically induced strain rates, is predominantly responsible for the generation/annihilation of curvature in the reaction zone and on the burnt side of the flame. On the contrary, the generation of mean curvature on the unburned side is governed by the flow stretching term $T_3 = -2(S_{ij} n_{j,i})$ and curvature generation by flow strain gradients $T_4 = -(\partial S_{ij}/\partial x_i)(n_j/2)$. The mean values of T_3 and T_8 conditioned upon the mean curvature k_m and Gauss curvature k_g indicate that the annihilation of flame curvature is prevalent at concave scalar iso-surfaces, whereas the generation of flame curvature occurs at convex scalar iso-surfaces. On the other hand, the added terms T_9 and T_{10} are the main contributions to the flame curvature for concave scalar iso-surfaces. The present study also reveals that the mean curvature within the flame and especially in the reaction zone is controlled by the balance between micro-mixing and combustion and future development of mixing models should incorporate some representation of mean curvature evolution to relate the coupling between small-scale flow strain rate, molecular diffusion and chemical conversion.

Acknowledgments

The authors are grateful to Jülich Supercomputing Centre (JSC), support by the state of NRW, EPSRC and ARCHER for financial and computational support. This project has received funding from the European Union's Horizon 2020 research and innovation program under grant agreement No 706672 - ITPF.

[1] P. Pelcé, Academic Press, Inc (1988).

[2] G. H. Markstein, Dynamics of Curved Fronts (1988) 413–423.

[3] P. Clavin, G. Joulin, Journal de Physique Lettres 44 (1983) 1–12.

[4] D. W. Mikolaitis, Combust. Flame 57 (1984) 25–31.

[5] D. W. Mikolaitis, Combust. Flame 58 (1984) 23–29.

[6] D. Haworth, T. Poinsot, J. Fluid Mech. 244 (1992) 405–436.

[7] C. Rutland, A. Trouvé, Combust. Flame 94 (1993) 41–57.

[8] T. Echekki, J. H. Chen, Combust. Flame 106 (1996) 184–202.

[9] B. Renou, A. Boukhalfa, D. Puechberty, M. Trinité, Symposium (International) on Combustion 27 (1998) 841–847.

[10] N. Peters, P. Terhoeven, J. H. Chen, T. Echekki, Symposium (International) on Combustion 27 (1998) 833–839.

[11] T. Echekki, J. H. Chen, Combust. Flame 118 (1999) 308–311.

[12] J. H. Chen, H. G. Im, Symposium (International) on Combustion 27 (1998) 819–826.

[13] J. B. Chen, H. G. Im, Proc. Combust. Inst. 28 (2000) 211–218.

[14] E. R. Hawkes, J. H. Chen, Combust. Flame 138 (2004) 242–258.

[15] E. R. Hawkes, J. H. Chen, Proc. Combust. Inst. 30 (2005) 647–655.

[16] N. Chakraborty, S. Cant, Combust. Flame 137 (2004) 129–147.

[17] N. Chakraborty, R. Cant, Phys. Fluids 17 (2005) 105105.

[18] N. Chakraborty, R. Cant, Phys. Fluids 17 (2005) 065108.

[19] K. Jenkins, M. Klein, N. Chakraborty, R. Cant, Combust. Flame 145 (2006) 415–434.

[20] M. Klein, N. Chakraborty, K. Jenkins, R. Cant, Phys. Fluids 18 (2006) 055102.

[21] V. R. Savarianandam, C. Lawn, Combust. Flame 146 (2006) 1–18.

[22] N. Chakraborty, Phys. Fluids 19 (2007) 105109.

[23] N. Chakraborty, E. Hawkes, J. Chen, R. Cant, Combust. Flame 154 (2008) 259–280.

[24] I. Han, K. Y. Huh, Combust. Flame 152 (2008) 194–205.

[25] G. Hartung, J. Hult, R. Balachandran, M. Mackley, C. Kaminski, Applied physics b 96 (2009) 843–862.

[26] N. Chakraborty, M. Klein, R. Cant, J. Combust. 2011 (2011).

[27] N. Chakraborty, G. Hartung, M. Katragadda, C. Kaminski, Combust. Flame 158 (2011) 1372–1390.

[28] J. Kerl, C. Lawn, F. Beyrau, Combust. Flame 160 (2013) 2757–2769.

[29] G. K. Giannakopoulos, M. Matalon, C. Frouzakis, A. G. Tomboulides, Proc. Combust. Inst. 35 (2015) 737–743.

[30] A. Marshall, J. Lundrigan, P. Venkateswaran, J. Seitzman, T. Lieuwen, Proc. Combust. Inst. 35 (2015) 1417–1424.

[31] A. Aspden, J. Bell, M. Day, F. Egolfopoulos, Proc. Combust. Inst. 36 (2017) 2005–2016.

[32] S. Pope, Int. J. Eng. Sci. 26 (1988) 445–469.

[33] S. M. Candel, T. J. Poinsot, Combust. Sci. Technol. 70 (1990) 1–15.

[34] L. Vervisch, E. Bidaux, K. Bray, W. Kollmann, Phys. Fluids 7 (1995) 2496–2503.

[35] N. Chakraborty, M. Klein, Phys. Fluids 20 (2008) 065102.

[36] N. Chakraborty, M. Klein, Proc. Combust. Inst. 32 (2009) 1435–1443.

[37] A. Sandeep, F. Proch, A. M. Kempf, N. Chakraborty, Phys. Fluids 30 (2018) 065101.

[38] S. Girimaji, S. Pope, J. Fluid Mech. 234 (1992) 247–277.

[39] Y. Gao, N. Chakraborty, N. Swaminathan, J. Combust. 2014 (2014).

[40] N. Chakraborty, R. Cant, Phys. Fluids 19 (2007) 105101.

[41] N. Chakraborty, R. Cant, Proc. Combust. Inst. 32 (2009) 1445–1453.

[42] Y. Gao, N. Chakraborty, N. Swaminathan, Combust. Sci. Technol. 187 (2015) 362–383.

[43] J. Kwon, Y. Park, K. Y. Huh, Combust. Flame 164 (2016) 85–98.

[44] M. Klein, N. Chakraborty, R. Cant, Flow Turbul. Combust. 81 (2008) 583–607.

[45] H. A. Uranakara, S. Chaudhuri, K. Lakshmisha, Proc. Combust. Inst. 36 (2017) 1793–1800.

[46] P. Clavin, F. Williams, Prog. Astronaut. Aeronaut 76 (1981) 403.

[47] G. I. Sivashinsky, Annual Review of Fluid Mechanics 15 (1983) 179–199.

[48] F. Creta, R. Lamioni, P. E. Lapenna, G. Troiani, Phys. Rev. E 94 (2016) 053102.

[49] I. Shepherd, W. T. Ashurst, Symposium (International) on Combustion 24 (1992) 485–491.

[50] W. T. Ashurst, I. Shepherd, Combust. Sci. Technol. 124 (1997) 115–144.

[51] T.-W. Lee, G. North, D. Santavicca, Combust. Sci. Technol. 84 (1992) 121–132.

[52] T.-W. Lee, G. North, D. Santavicca, Combust. Flame 93 (1993) 445–456.

[53] S. Gashi, J. Hult, K. W. Jenkins, N. Chakraborty, S. Cant, C. F. Kaminski, Proc. Combust. Inst. 30 (2005) 809–817.

[54] F. T. Yuen, Ö. L. Gülder, Proc. Combust. Inst. 32 (2009) 1747–1754.

[55] H. Wang, E. R. Hawkes, B. Zhou, J. H. Chen, Z. Li, M. Aldén, Proc. Combust. Inst. 36 (2017) 2045–2053.

[56] C. Dopazo, J. Martin, L. Cifuentes, J. Hierro, Flow Turbul. Combust. (2018) 1–32.

[57] F. Proch, P. Domingo, L. Vervisch, A. M. Kempf, Combust. Flame 180 (2017) 321–339.

[58] M. S. Sweeney, S. Hochgreb, M. J. Dunn, R. S. Barlow, Combust. Flame 159 (2012) 2896–2911.

[59] M. S. Sweeney, S. Hochgreb, M. J. Dunn, R. S. Barlow, Combust. Flame 159 (2012) 2912–2929.

[60] R. Zhou, S. Balusamy, M. S. Sweeney, R. S. Barlow, S. Hochgreb, Combust. Flame 160 (2013) 2017–2028.

[61] M. Euler, R. Zhou, S. Hochgreb, A. Dreizler, Combust. Flame 161 (2014) 2842–2848.

[62] M. M. Kamal, R. Zhou, S. Balusamy, S. Hochgreb, Proc. Combust. Inst. 35 (2015) 3803–3811.

[63] M. M. Kamal, R. S. Barlow, S. Hochgreb, Combust. Flame 162 (2015) 3896–3913.

[64] C. Dopazo, L. Cifuentes, J. Martin, C. Jimenez, Combust. Flame 162 (2015) 1729–1736.

[65] C. Dopazo, L. Cifuentes, J. Hierro, J. Martin, Flow Turbul. Combust. 96 (2016) 547–571.

[66] C. Dopazo, L. Cifuentes, Combust. Sci. Technol. 188 (2016) 1376–1397.

[67] C. Dopazo, J. Martin, J. Hierro, Phys. Rev. E. 76 (2007) 056316.

[68] R. Mercier, B. Fiorina, F. Proch, A. M. Kempf, TSFP Digital Library Online (2013).

[69] R. Mercier, T. Schmitt, D. Veynante, B. Fiorina, Proc. Combust. Inst. 35 (2015) 1259–1267.

[70] F. Proch, A. M. Kempf, Combust. Flame 161 (2014) 2627–2646.

[71] B. Fiorina, O. Gicquel, L. Vervisch, S. Carpentier, N. Darabiha, Combust. Flame 140 (2005) 147–160.

[72] P.-D. Nguyen, L. Vervisch, V. Subramanian, P. Domingo, Combust. Flame 157 (2010) 43–61.

[73] J. v. Oijen, L. d. Goey, Combust. Sci. Technol. 161 (2000) 113–137.

[74] N. Peters, Turbulent combustion, Cambridge university press, 2000.

[75] M. Boger, D. Veynante, H. Boughanem, A. Trouvé, Symposium (International) on Combustion 27 (1998) 917–925.

[76] N. Chakraborty, N. Swaminathan, Phys. Fluids 19 (2007) 045103.

[77] G. Hartung, J. Hult, C. Kaminski, J. Rogerson, N. Swaminathan, Phys. Fluids 20 (2008) 035110.

[78] L. Cifuentes, C. Dopazo, J. Martin, P. Domingo, L. Vervisch, Proceedings of the Combustion Institute 35 (2015) 1295–1303.

[79] C. Dopazo, in Turbulent reacting flows (1994) 375–474.